12,16

Atomic structures and growth of monoanion germanium-vanadium glusters VGe_n^- ($n = 5-19$): analysis based on the Wade–Mingos rule

© N.A. Borshch[1], N.S. Pereslavtseva[1], S.I. Kurganskii[2]

[1] Voronezh State Technical University,
Voronezh, Russia
[2] Voronezh State University,
Voronezh, Russia

E-mail: n.a.borshch@ya.ru

Received May 5, 2022
Revised May 17, 2022
Accepted May 18, 2022

The paper presents the results of calculations of the spatial structure and electronic spectra of various isomers of anionic vanadium-germanium clusters VGe_n^- ($n = 5-19$). The calculations were carried out using three functionals — B3LYP, B3PW91 and PBE in combination with the 6-311 + $g(d)$ basis set. Interpretation of the results of calculations of the spatial structure of clusters using data from their photoelectron spectroscopy made it possible to solve two problems at once. First, perform a Wade–Mingos rule test for a given set of clusters. Secondly, to eliminate errors in the analysis of the results and to establish the spatial structure of clusters with the greatest reliability.

Keywords: atomic clusters, density functional theory, Wade–Mingos rule, electronic spectrum.

DOI: 10.21883/PSS.2022.10.54248.372

1. Introduction

Atomic clusters have been the object of close attention of researchers for several decades [1–20]. They are interesting both as independent zero-dimensional objects, and as elementary blocks for the construction of nanostructured materials of various dimensions [21–25]. For the predictive design of new nanoforms, it is necessary to have reliable information about the spatial structure of clusters, as well as to understand the mechanisms of their formation.

One of the main problems in the study of atomic clusters is the inability to reliably determine their spatial structure. Experimental methods currently cannot provide such information, so the main source of information is a computer experiment. For optimization calculations of the spatial structure of clusters, various methods are most often used within the framework of density functional theory. However, it turns out that the results of such calculations can radically depend on the functional used [26]. There is a situation when theoretical studies give ambiguous and often unconfirmed results. At the same time, an experimental study of the electronic structure of clusters is possible, and works are known in which the results of the study of the electron energy spectrum of anionic clusters by photoelectronic spectroscopy are presented [27–30]. One of the effective methods for determining the actual spatial structure of clusters is the method of combining the results of computer modeling of stable structures with the results of photoelectronic spectroscopy [31–37]. This approach makes it possible to obtain data on the spatial structure of clusters — first, the spatial structure is optimized by theoretical methods, then the calculation of the electronic spectrum of optimized structures is carried out, on the basis of which experimental photoelectronic spectra are modeled and the calculated spectra are compared with experimental ones.

There are several approaches to explain the increased stability of some silicon-metal clusters, which are often referred to as „magic“. Firstly, it is a hypothesis about the fulfillment of the rule of 18 or 20 electrons [38], according to which a quasi-free electron gas is considered in clusters, where each silicon atom gives up one valence electron, and the metal atom — all valence electrons, including d-electrons. The most stable were those silicon-metal clusters that contain 18 quasi-free electrons (the rule of 18 electrons) or 20 free electrons (the rule of 20 electrons). The second approach is the concept of „superatoms“ [39,40], in which quasi-free electrons in the cluster are considered to fill the cluster orbitals. Filling such orbitals in the most stable clusters is analogous to filling the atomic orbitals of some elements — halogens, alkaline earth metals, noble gases, etc.

These approaches help explain the stability of some „magic“ clusters compared to other clusters with the same qualitative composition. However, until now, no patterns have been studied that would allow us to describe the formation of clusters as the number of atoms in them increases. The establishment of such patterns will significantly improve the accuracy of the interpretation of the results of a computer experiment, which is especially important in the case when there is no experimental data for comparison.

One approach that allows you to predict the structures of clusters is the Wade–Mingos rule approach. These rules were formulated for the borans and carboranes by K. Wade [41], and later supplemented by M. Mingos [42]. They make it possible to establish a connection between the number of valence electrons in the cluster and the features of its spatial structure. According to the $4n$-modification of the Wade–Mingos rule, the structure of clusters in which there are four electrons per vertex is a deltahedral polyhedron of one of three types — *arachno, nido* or *closo* [41,42]. If the number of valence electrons in a cluster with n vertices obeys the condition of $4n + 6$, its structure must be an arachno-polyhedron, which is obtained by removing two vertices from a closo-polyhedron with $n + 2$ vertices.

This paper considers the possibility of applying the Wade–Mingos rules to describe the growth process of anionic vanadium-germanium clusters VGe_n^- ($n = 5-19$), for which the condition of $4n + 6$ valence electrons per cluster is met. The results of calculations of the spatial structure and electron spectra of various isomers of anionic vanadium-germanium clusters VGe_n^- ($n = 5-19$) are presented. Calculations were carried out using three functionals — B3LYP [43,44], B3PW91 [45] and PBE [46,47] in combination with the basis 6-311 + $g(d)$ [48,49]. For calculations, the Gaussian 09 program was used [50]. The use of three functionals made it possible to identify the features of each of them in the optimization calculations of the spatial structure of clusters and to eliminate errors in the interpretation of the results as much as possible. Interpretation of the results of calculations of the spatial structure of clusters with the help of data on their photoelectronic spectroscopy made it possible to solve two problems at once — firstly, to check the implementation of the Wade–Mingos rule for this series of clusters, and secondly, to investigate the dependence of the results of optimization calculations of the spatial structure of clusters on the functional used.

The atomic structure and electronic properties of some anionic [51–53] and neutral [54] vanadium-germanium clusters have been studied earlier. However, each of the works has a number of significant features that do not allow us to assert the full adequacy of the results presented there. Thus, in the studies [51,52] for optimization calculations of the atomic structure and the search for the major isomers, the B3LYP functional [51] or BP86 functional [52] in combination with the LANL2DZ basis is used. As we showed earlier [26], the use of B3LYP functional can lead to significant errors in estimating the relative binding energies of various isomers. In addition, the LANL2DZ basis is a valence basis, not a full-electron basis, which also does not include diffuse functions [55], which can also lead to inaccurate results in the calculation of anionic systems. The authors [53] give in their work the photoelectronic spectra of the VGe_n^- clusters ($n = 3-12$) and the results of optimization calculations of their atomic structure, but do not give the results of the calculated electron spectra of each isomer and, accordingly, cannot compare them with experimental spectra. Therefore, the results of calculations of atomic structures presented in [53] have not been confirmed experimentally. The same drawback can be noted in the work [54], which presents the results of the calculation of the atomic structures of neutral germanium-vanadium clusters. The results presented there have no experimental confirmation, and are also carried out using only one PBE functional, which can lead to significant errors in interpretation [26]. All this once again confirms the need to search for a single pattern describing the formation of germanium-metal clusters.

2. Calculation procedure

As a result of the calculation, the eigenvalues of the energy of each molecular orbital were obtained, i.e. the energy spectrum in which each molecular orbital can be represented as a level. Theoretical spectra were obtained after each energy level was replaced by a Gaussian distribution with a half-width of 0.15 eV and the intensities of all distributions at each energy value were added. The combination of calculated and experimental spectra on the energy scale was carried out according to the position of the upper filled orbital.

The mean bond energy was calculated by the formula

$$E_b = \frac{nE(\mathrm{Ge}) + E(\mathrm{V}^-) - E(\mathrm{VGe}_n^-)}{n+1},$$

where $E(\mathrm{Ge})$ and $E(\mathrm{V}^-)$ — the total energies of the free atom of germanium and the vanadium anion, respectively, $E(\mathrm{VGe}_n^-)$ — the total energy of the cluster, n — the number of atoms of germanium in the cluster.

3. Results and discussion

Figures 1–5 show the spatial structures of the major isomers of VGe_n^- clusters ($n = 5-19$) and compare the calculated electron spectra of all isomers of each cluster with the corresponding photoelectronic spectrum [30]. The table below shows the differences in the average binding energies between the major isomer and the rest for all three calculations.

VGe_5^-. Cluster VGe_5^- has the structure of a quadrangular bipyramid with a vanadium atom at one of the vertices. The main state of the cluster according to the results of all calculations is the spin-triplet state. However, in the B3PW91 calculation, the average binding energies of the spin-singlet and spin-triplet states of this isomer are close, and experimental observation of the cluster in these both states can be assumed. Figure 2 shows that the best agreement with the experimental photoelectronic spectrum [30] shows the calculated electron spectrum of the cluster in the spin-triplet state, as well as the total spectrum of the cluster in the spin-singlet and spin-triplet

states. The calculated spectrum of the VGe_5^- cluster in the spin-singlet state is less consistent with the experimental spectrum. This confirms the assumption made on the basis of the B3PW91 calculation that both cluster states were experimentally detected.

VGe_6^-. Cluster VGe_6^- has the structure of a pentagonal bipyramid with a vanadium atom at one of their vertices. The main state, according to all calculations, is spin-triplet, but the average binding energies in the spin-singlet and spin-quintet states are slightly less, so it is possible to allow the observation of all three multiplet states of this structure in the experiment. This assumption is confirmed by a comparison of calculated and experimental [30] electron spectra.

VGe_7^-. The major isomer of the VGe_7^- cluster is obtained by adding an additional germanium atom to a bipyramid identical to the VGe_6^- cluster structure. The extra atom forms two Ge−Ge bonds and one Ge−V bond. The average binding energies in all three multiple states are close in all calculations, so all states can be detected experimentally. As can be seen from Fig. 2, the comparison of the calculated and experimental [30] spectra confirms this.

VGe_8^- −VGe_{10}^-. For clusters, the major ones are isomers, the structures of which are obtained after removing two vertices from the *closo*-polyhedron with $n+2$ vertices, i.e. *arachno*-structure (Fig. 1). According to the results of all calculations, the average binding energies in these isomers are much greater than in other isomers, and the comparison of the calculated electron spectra with the photoelectronic [30] shows the complete coincidence of their profiles (Fig. 2). All this gives grounds to assert that such isomers were detected experimentally.

VGe_{11}^-. The two most stable cluster isomers VGe_{11}^- 11-ARH1 and 11-ARH2 are obtained after removing two vertices from *closo*-polyhedron with thirteen vertices. The mean bond energy in the isomer 11-ARH1 is higher than in 11-ARH2, but the difference between the energies is such that it is possible to allow the observation of both structures in the experiment. Comparing their electron spectra with the photoelectronic one [30] shows an almost perfect agreement for the spectrum of the major isomer 11-ARH1. The spectrum of the isomer 11-ARH2 is worse consistent with the experimental one due to the pronounced maximum at the ceiling of the valence band (see Fig. 2). In the total spectrum of isomers, this maximum is smoothed out and it can be argued that the total spectrum agrees well with the experimental one. This supports the assumption, based on calculation data, that both isomers can be detected experimentally.

VGe_{12}^-. The reliable determination of the atomic structure of the VGe_{12}^- cluster is of particular interest, since it is assumed that it can have a prism or antiprism structure and serve as a building unit for the formation of larger nanoobjects.

The isomers 12-PR and 12-APR have the shape of a hexagonal prism and antiprism, respectively, with a vanadium atom in the center. The isomers 12-ARH1 and

The differences in the average binding energies (eV/at.) between the major isomer and the rest for all three calculations

Cluster	Isomer	B3LYP	B3PW91	PBE
VGe_5^{-1}	$2S+1=1$	0.0143	0.0081	0.0241
	$2S+1=3$	0.0000	0.0000	0.0000
	$2S+1=5$	0.0156	0.0147	0.0138
VGe_6^-	$2S+1=1$	0.0108	0.0108	0.0054
	$2S+1=3$	0.0000	0.0000	0.0000
	$2S+1=5$	0.0036	0.0036	0.0103
VGe_7^-	$2S+1=1$	0.0026	0.0087	0.0106
	$2S+1=3$	0.0000	0.0000	0.0000
	$2S+1=5$	0.0098	0.0080	0.0089
VGe_{11}^-	11-ARH1	0.0000	0.0000	0.0000
	11-ARH2	0.0125	0.0165	0.0151
VGe_{12}^-	12-ARH1	0.0287	0.0223	0.0000
	12-ARH2	0.0386	0.0346	0.0145
	12-PR	0.0000	0.0000	0.0064
	12-APR	0.0218	0.0140	0.0007
VGe_{13}^-	13-ARH1	0.0000	0.0000	0.0000
	13-ARH2	0.0368	0.0262	0.0318
	13-PR	0.0662	0.0600	0.0748
VGe_{14}^-	14-ARH1	0.0000	0.0000	0.0000
	14-ARH2	0.0292	0.0381	0.0339
VGe_{15}^-	15-ARH1	0.0035	0.0000	0.0000
	15-ARH2	0.0038	0.0017	0.0030
	15-ARH3	0.0111	0.0048	0.0046
	15-ARH4	0.0486	0.0510	0.0529
	15-ARH5	0.0158	0.0268	0.0317
	15-PR1	0.0000	0.0110	0.1070
	15-PR2	0.0511	0.0831	0.0202
VGe_{16}^-	16-ARH1	0.0004	0.0000	0.0000
	16-ARH2	0.0041	0.0004	0.0021
	16-ARH3	0.0188	0.0141	0.0114
	16-FK	0.0167	0.0132	0.0095
	16-PR	0.0000	0.0006	0.0062
VGe_{17}^-	17-ARH1	0.0127	0.0006	0.0000
	17-ARH2	0.0144	0.0068	0.0065
	17-ARH3	0.0208	0.0083	0.0026
	17-FULL	0.0081	0.0097	0.0184
	17-PR	0.0000	0.0000	0.0040
VGe_{18}^-	18-ARH1	0.0000	0.0000	0.0000
	18-ARH2	0.0145	0.0126	0.0011
	18-ARH3	0.0372	0.0301	0.0130
	18-FULL	0.0460	0.0627	0.0735
	18-PR	0.0234	0.0244	0.0213
VGe_{19}^-	19-ARH1	0.0000	0.0000	0.0000
	19-ARH2	0.0046	0.0041	0.0044
	19-FULL1	0.0226	0.0338	0.0514
	19-FULL2	0.0281	0.0407	0.0467
	19-PR	0.0205	0.0076	0.0365

12-ARH2 can be thought of as *arachno*-structures. They are obtained by removing two vertices from *closo*-polyhedron with fourteen vertices (see Fig. 1).

The major isomer according to the results of B3LYP and B3PW91 calculations is the prismatic isomer of 12-PR. The remaining isomers have a noticeable energy gap from this structure, which may lead to the conclusion that their observation in the experiment is much less likely. However, according to the results of the PBE calculation, the highest values of the average binding energy correspond to the structures of 12-APR and 12-ARH1. The mean bond energy in the isomer of 12-PR in this calculation is slightly less than that of the most stable structures, so its existence is no less likely.

By comparing the calculated electron spectra of isomers with the experimental photoelectronic, it is possible to determine which of the optimization methods gives a more adequate result. Figure 3 shows that the profile of the electron spectrum in the prismatic isomer of 12-PR does not correspond well to the profile of the experimental spectrum. The critical difference is, first of all, the presence of a pronounced maximum in the calculated spectrum at the ceiling of the band of filled states, which is not present in the experimental spectrum. Therefore, it can reasonably be concluded that the observation of the prismatic isomer in the experiment, if possible, is only together with other structures. To verify this, you should consider the total spectra of different isomers. Thus, the total spectrum of the isomer 12-PR and the isomer of 12-APR, which is the second most stable in the B3PW91 calculation, is better consistent with the experimental one, since in this spectrum the maximum has a much lower intensity. The best agreement with the experiment is shown by the total range of isomers of 12-APR and 12-ARH1, which are the major ones in optimization calculations using PBE functional. This spectrum corresponds to the experimental one both in the number of expressed maxima and in the ratio of intensities between them. Since the prismatic isomer also has a high stability in the PBE calculation, Fig. 3 also shows the total spectrum of the three isomers — 12-APR, 12-ARH1 and 12-PR. Obviously, the presence of a high-energy maximum from the contribution to the spectrum of the isomer of 12-PR, makes it less similar to the experimental one. However, it should be borne in mind that in the total spectrum, for simplicity, an equal contribution from the electron spectra of all isomers is assumed, and in reality the number of prismatic isomers may be less due to the lower average binding energy in them (according to the results of the PBE calculation). This could lead to a small influx in the experimental spectrum. Therefore, experimental detection of prismatic structures cannot be ruled out. Summarizing, it can be noted that the most likely experimental observation of three types of isomers is — 12-APR, 12-ARH1 and 12-PR.

It can be noted that the above results of optimization calculations of VGe_n^- clusters ($n = 5-2$) are generally consistent with those presented in [53], but in some details differ from [51,52]. Comparison with the experimental photoelectron spectrum [30] in a relatively wide energy interval compared to the experiment [53], as well as a comparative analysis of the results obtained using three different functionals, allow us to clarify and supplement the results from [53]. In particular, we have shown that in an experiment several isomers of the same atomic composition with close binding energies can be detected at once.

VGe_{13}^-. Isomers 13-ARH1 and 13-ARH2 are *arachno*-polyhedra, that is, they are derived from *closo*-polyhedron with fifteen vertices after the removal of two vertices (see Fig. 1). The isomer 13-ARH2 can also be thought of as a hexagonal antiprism with an additional germanium atom that forms four Ge−Ge bonds with one of the bases of the antiprism. The prismatic isomer 13-PR has the structure of a distorted hexagonal prism with an additional germanium atom that forms Ge-Ge bonds with atoms of one of the prism bases.

All three optimization calculations for the VGe_{13}^- cluster showed the same result — the major isomer is the 13-ARH1 isomer. The second most stable is also *arachno*-structure — isomer 13-ARH1. According to the results of B3PW91 and PBE calculations, the energy separation of this isomer from the major one is such that its observation in the experiment cannot be ruled out, but it can be assumed that such structures are small in the total mass of those detected experimentally. Upon the results of the B3LYP calculation, it can be concluded that the isomer 13-ARH1 is most likely the only one observed experimentally.

A comparison of the calculated electron spectra with the experimental one (see Fig. 3) confirms this conclusion. The best correspondence to the experimental one is the electron spectrum of the isomer 13-ARH1. The spectrum of the isomer 13-ARH2 is somewhat worse, since in the spectrum of this isomer there is a pronounced maximum at the ceiling of the valence state band, which is weakly expressed in the experimental spectrum. However, in the total spectrum of isomers 13-ARH1 and 13-ARH2, this feature is smoothed out and the correspondence to the experimental one is much better. The profile of the electronic spectrum of the 13-PR isomer has radical differences with the profile of the photoelectronic spectrum, so the probability of detecting it experimentally is extremely small.

VGe_{14}^-. The two most stable isomers have been obtained for the VGe_{14}^- cluster. Both of them have the structure of arachno-polyhedra, which are obtained by removing two vertices from the lateral surface of a closo-polyhedron with sixteen vertices (see Fig. 1). In the formation of the isomer 14-ARH1, two vertices are removed from the lateral surface of the closo-polyhedron, and the isomer 14-ARH2 is obtained by removing two vertices at one of its bases. The major isomer according to the results of all three calculations with a large energy margin is the isomer 14-ARH1.

Comparison of the calculated electron spectrum of the isomers 14-ARH1 and 14-ARH2 with the experimental one [30] shows that the spectral profiles of both isomers

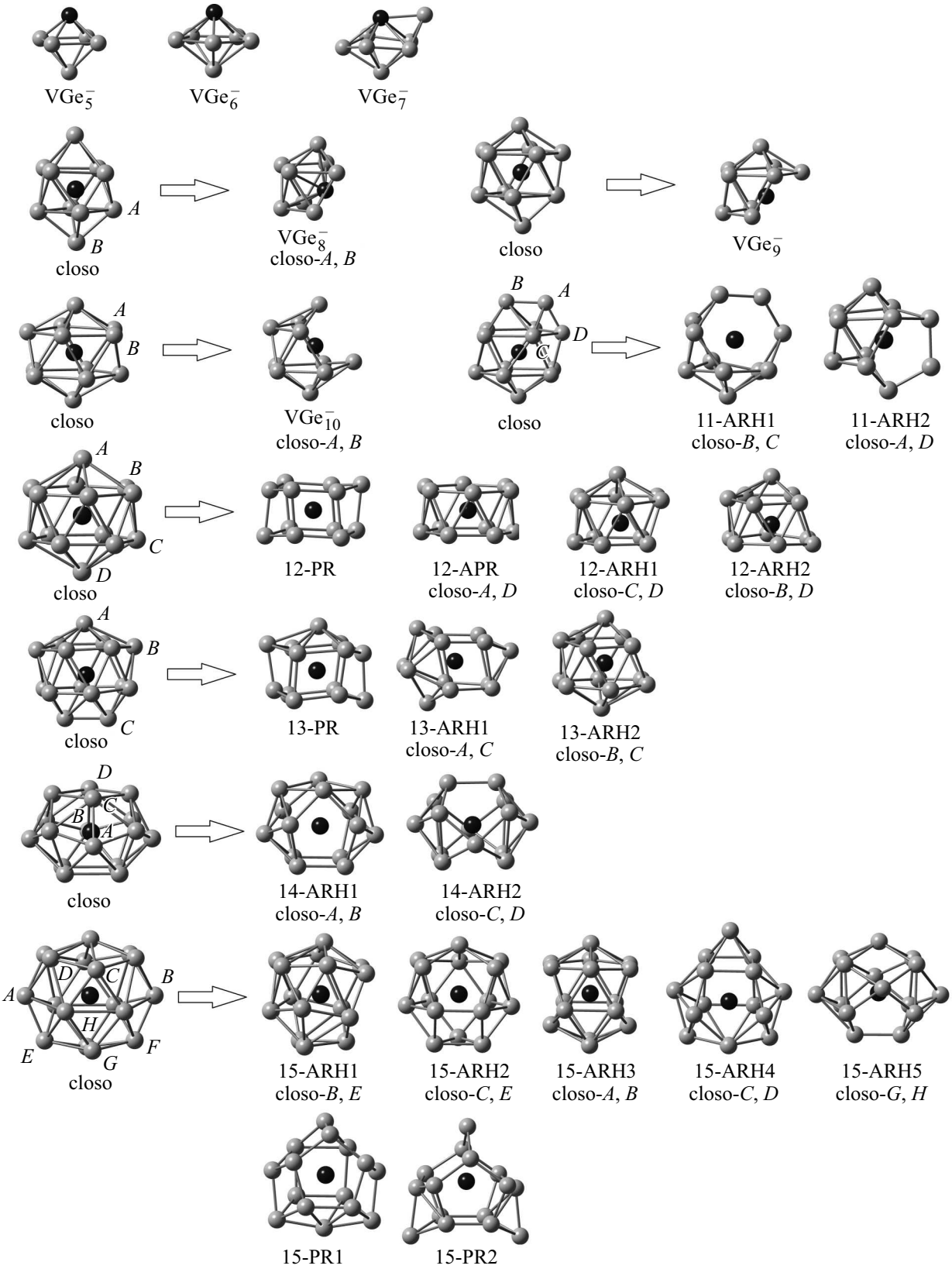

Figure 1. Spatial structures of stable isomers of clusters ($n = 5-15$). Germanium atoms are shown in gray, and vanadium atom is shown in black. V−Ge bonds in closed structures are not shown to simplify the figure.

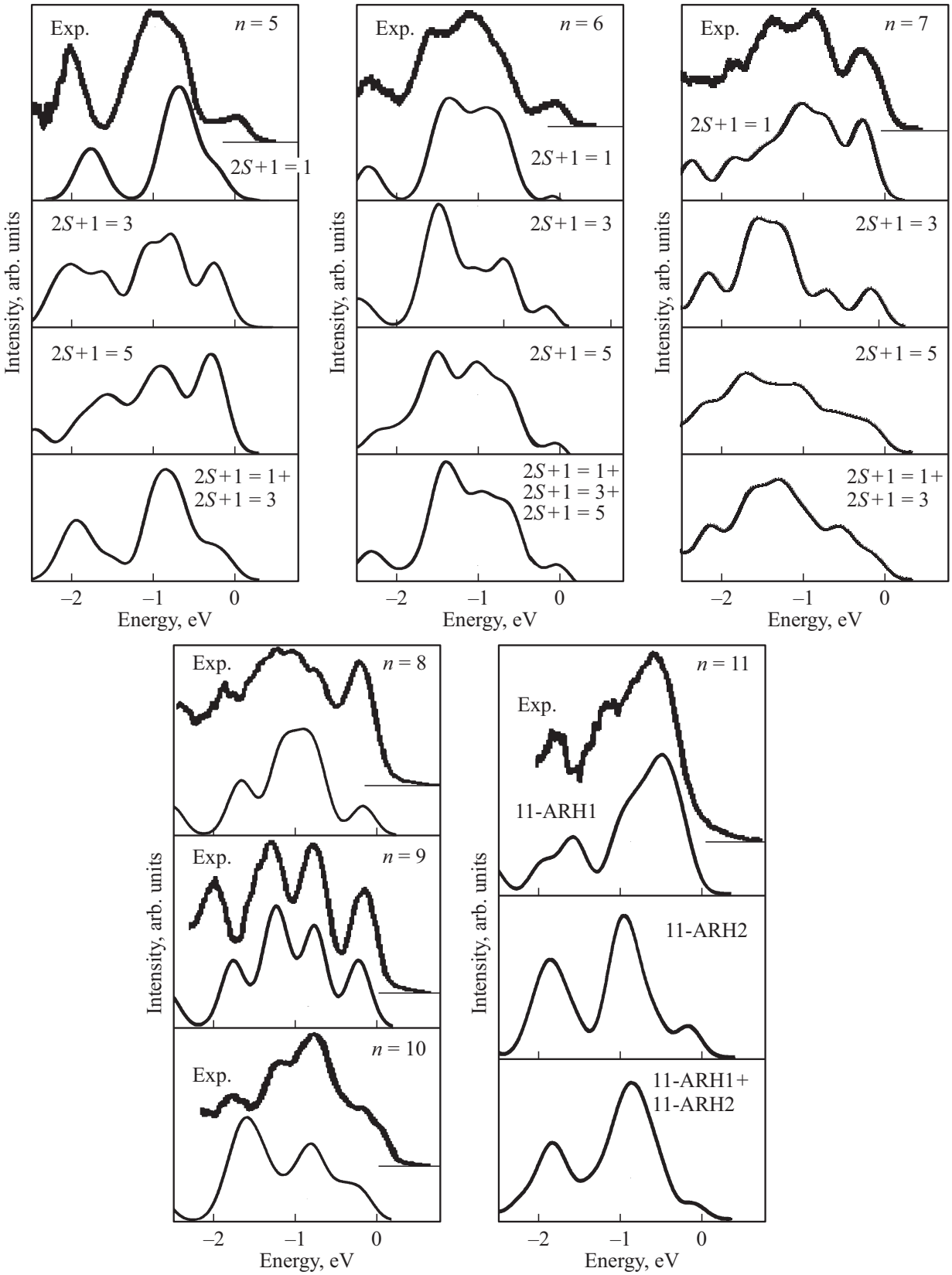

Figure 2. Computation of calculated electron spectra of clusters ($n = 5-11$) with the experimental photoelectronic spectrum [30].

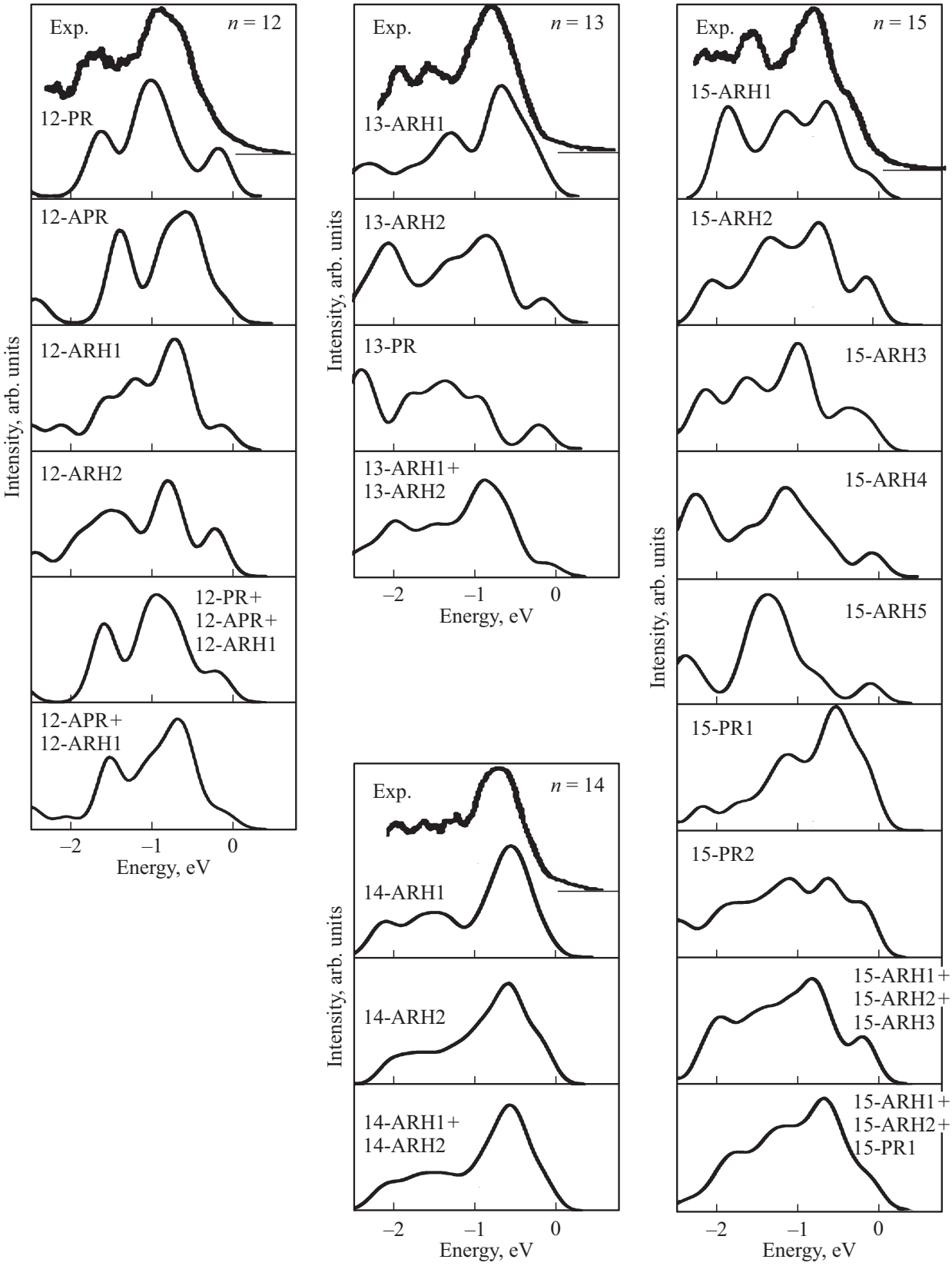

Figure 3. Computation of calculated electron spectra of clusters ($n = 12-15$) with the experimental photoelectronic spectrum [30].

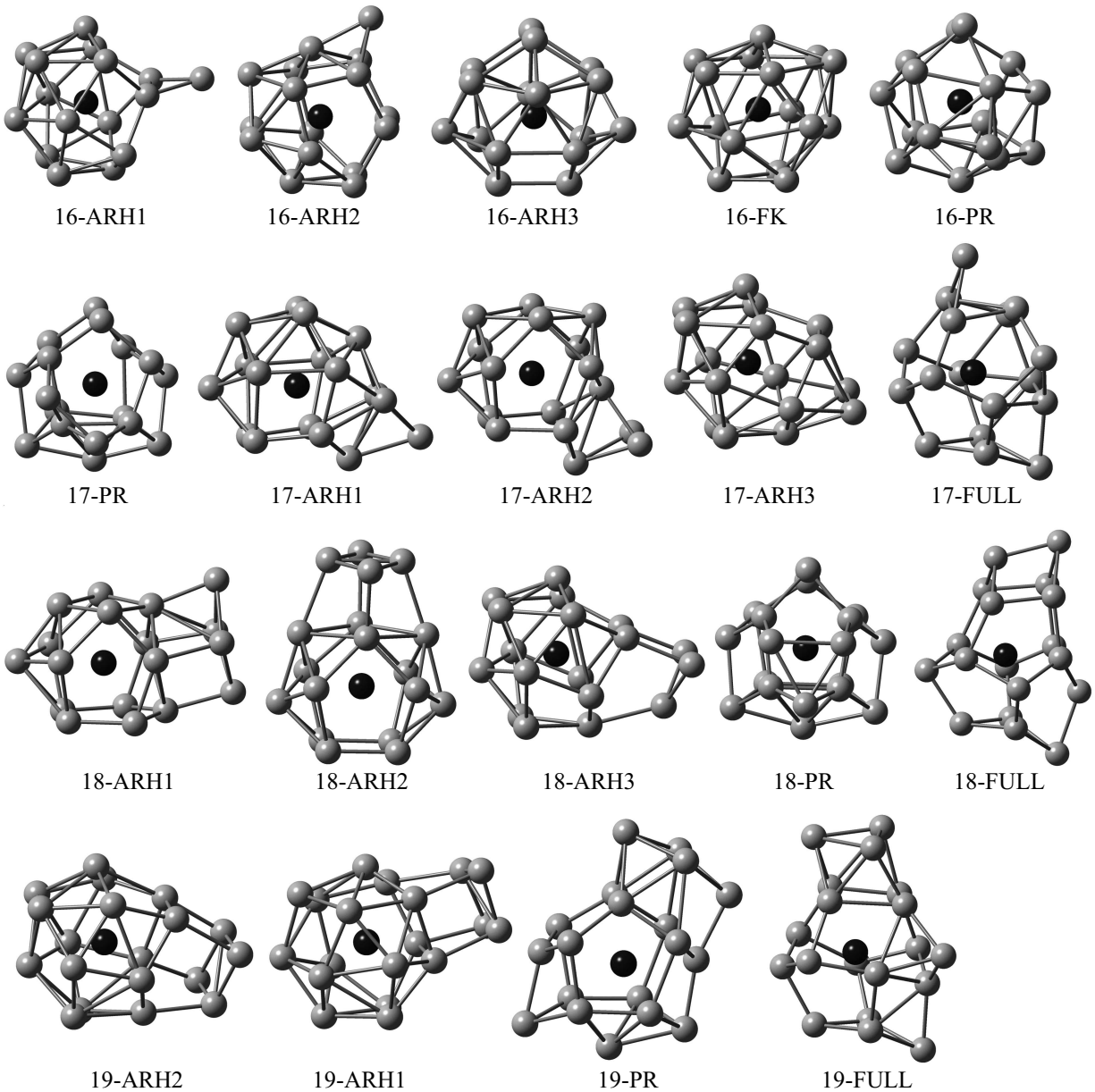

Figure 4. Space structures of stable isomers of clusters ($n = 16-19$). Germanium atoms are shown in gray, and vanadium atom is shown in black. V−Ge bonds in closed structures are not shown to simplify the figure.

correspond with high accuracy to the profile of the photoelectronic spectrum, as well as the profile of their total spectrum. This fact does not exclude the possibility of experimental observation of both the isomer 14-ARH1 and the isomer 14-ARH2, despite the fact that according to the results of optimization calculations, the mean bond energy of 14-ARH2 is much less.

VGe_{15}^-. Five cluster isomers can be thought of as *arachno*-polyhedra obtained after removing two vertices from *closo*-polyhedron with seventeen vertices. These are the isomers 15-ARH1, 15-ARH2, 15-ARH3, 15-ARH4 and 15-ARH5. The scheme of their formation is shown in Fig. 1. The isomers 15-PR1 and 15-PR2 basically have a distorted hexagonal prism with a vanadium atom inside. In the isomer 15-PR1, all three additional germanium atoms form bonds with one prism base, and in the 15-PR2 isomer, one of the additional atoms is located above the opposite base relative to the other two.

In calculations using the B3PW91 and PBE functionals, the highest values of the average binding energy correspond to ARH isomers. All *arachno*-structures have almost equal average binding energies, so three isomers can be considered the major isomers of the VGe_{15}^- cluster. The values of the binding energies in the isomers 15-ARH4 and 15-ARH5 are significantly less than in other arachno-isomers, so it can be concluded that it is unlikely to experimentally obtain such clusters. The prismatic isomer 15-PR2 has a small energy gap from the major isomers, so

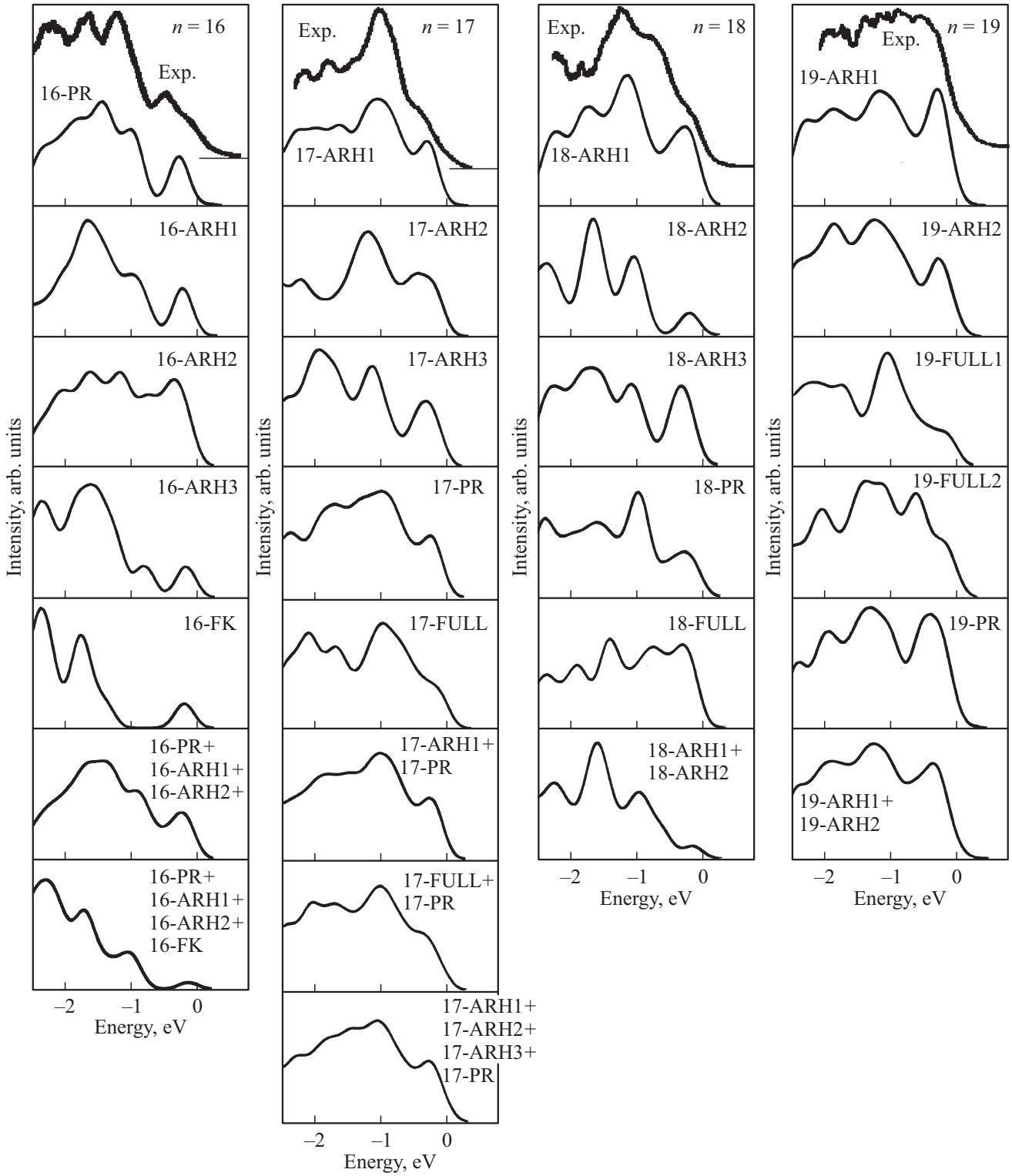

Figure 5. Computation of calculated electron spectra of clusters ($n = 16-19$) with the experimental photoelectronic spectrum [30].

the possibility of its existence cannot be ruled out. Another prismatic isomer, 15-PR1, has a radically lower average binding energy, making it nearly impossible to observe in an experiment. In the B3LYP calculation, the isomers 15-ARH1, 15-ARH2 and the prismatic isomer 15-PR2 have actually equal binding energies, the largest of all, i.e. these three structures in the B3LYP calculation are the main states of the cluster VGe_{15}^{-}.

Figure 3 shows the calculated densities of electronic states in all the described isomers of the VGe_{15}^{-} cluster and their

comparison with the experimental spectrum [30]. The density profiles of electronic states obtained in calculations with different functionals have practically no visible differences, so Fig. 3 shows the calculated electron spectra based on the results of the B3PW91 calculation. The calculated spectra of 15-ARH1, 15-ARH2 and 15-ARH3 isomers are consistent with the experimental spectrum. The profile of their total spectrum also corresponds to the profile of the experimental photoelectronic spectrum. This confirms the conclusions drawn from the results of B3PW91 and PBE calculations. The calculated spectrum of the isomer 15-PR2 is worse consistent with the experimental one, but the total spectrum of isomers 15-ARH1, 15-ARH2 and 15-PR2 shows good agreement. Summarizing all the described results, it can be concluded that it is experimentally possible to obtain four different isomers of the $VeGe_{15}^-$ cluster, three isomers with an arachno-structure and one prismatic isomer.

VGe_{16}^-. Isomers 16-ARH1 and 16-ARH2 are obtained by adding an additional germanium atom to structures similar to the isomers 15-ARH1 and 15-ARH2, respectively (see Fig. 4). The isomer 16-FK was obtained as a result of optimizing the original structure of a regular Frank–Casper polyhedron with sixteen vertices and a vanadium atom in the center. The optimized structure is distorted in such a way that for one of the germanium atoms the distance V-Ge significantly greater than for the others (3.60 Å against 2.67–3.15 Å according to the results of optimization using the B3PW91 method). The isomer 16-PR obtained by optimizing the original structure of a regular fullerene-like polyhedron. As a result, the polyhedron transformed into a prismatic structure identical to the structure of the isomer 15-PR2 with an additional germanium atom. The extra atom forms bonds with the front face of this prismatic structure, and the structure itself is markedly distorted.

All three optimization calculations showed that three isomers have almost equal average binding energies — isomers 16-ARH1 and 16-ARH2 and an isomer 16-PR and can be considered the major ones. The mean bond energy in the isomer 16-FK somewhat less than in these three, but the energy gap is small and on the basis of calculations allows us to assume that this structure can be detected experimentally.

As the comparison of the calculated electron spectra of all these isomers with the experimental one shows (Fig. 5), in none of them does the density profile of the electronic states fully correspond to the profile of the photoelectronic spectrum. The worst agreement with the experiment in the calculated spectrum of the isomer 16-FK due to the presence of a characteristic feature at the ceiling of the strip of occupied states.

VGe_{17}^-. Isomers 17-ARH1 and 17-ARH2 have the structure of a polyhedron similar to the polyhedron 14-ARH1 with three additional germanium atoms. The isomer 17-ARH3 — polyhedron similar to the 15-ARH2 isomer with two additional germanium atoms. The isomer 17-PR has a structure similar to that of the isomer 16-PR2. It is obtained by adding additional germanium atoms to the prismatic isomer 15-PR2. For the VGe_{17}^- cluster, the 17-FULL isomer was also stable, having the structure of a distorted fullerene-like polyhedron with sixteen vertices and with an additional germanium atom.

According to the results of the B3LYP calculation, the major isomers are 17-PR and 17-FULL. They have a significant energy gap from the rest of the structures, and it can be assumed that the existence of the remaining structures is unlikely. Optimization using B3PW91 functional shows that the major isomers are 17-PR and 17-ARH1 with almost equal average binding energies. The remaining isomers in the B3PW91 calculation also have virtually equal average binding energies, with a small energy gap from the major isomers. According to the results of the PBE calculation, all isomers, except for the isomer 17-FULL, can be considered major, and therefore equally probable detectable experimentally, since they have close values of the average binding energies. The isomer 17-FULL in this calculation is significantly less stable than the rest.

Comparison of the calculated electron spectra with the photoelectron spectrum [30] shows that the spectra of all isomers, except for the isomer 17-ARH3, agree well with the experimental one. In addition, we can note a good coincidence of the profiles of the total spectra of isomers 17-PR and 17-FULL, which are the major ones in the B3LYP calculation, the profiles of the sum of the spectra of isomers 17-PR and 17-ARH1, the major ones in the B3PW91 calculation, as well as the total spectrum of all isomers. It can be concluded that all the described isomers could be detected experimentally.

VGe_{18}^-. Isomers 18-ARH1 and 18-ARH2 are obtained by adding additional germanium atoms to a polyhedron identical to the *arachno*-polyhedron 14-ARH1. In the isomer 18-ARH1, four additional germanium atoms form bonds with one of the bases of the polyhedron, and in the isomer 18-ARH2 — with the atoms of the side faces. The 18-ARH3 isomer is obtained by adding additional germanium atoms to a polyhedron similar to the 15-ARH4 isomer. The prismatic isomer 18-PR is constructed similarly to the isomers 16-PR2 and 17-PR — adding additional germanium atoms to a polyhedron identical to the 15-PR1 isomer. Just as in the isomers 16-PR2 and 17-PR, additional atoms form bonds with the front face of this polyhedron. The fullerene-like isomer 18-FULL at the heart of its structure has a distorted fullerene-like polyhedron with sixteen vertices. Two additional germanium atoms form bonds of Ge–Ge with one of its bases.

The major isomer according to the results of B3LYP and B3PW91 calculations is the isomer 18-ARH1 with a noticeable energy gap from the rest. Optimization calculation using PBE functional shows that the average binding energies in the isomers 18-ARH1 and 18-ARH2 are almost equal. The isomers 18-ARH3 and 18-PR, according to the results of all three calculations, have noticeably lower binding energies, and the least stable isomer was 18-FULL. An almost perfect agreement with the experimental can be noted both for the total spectrum of isomers 18-ARH1 and 18-ARH2, and for the spectra of each of them separately (see Fig. 5).

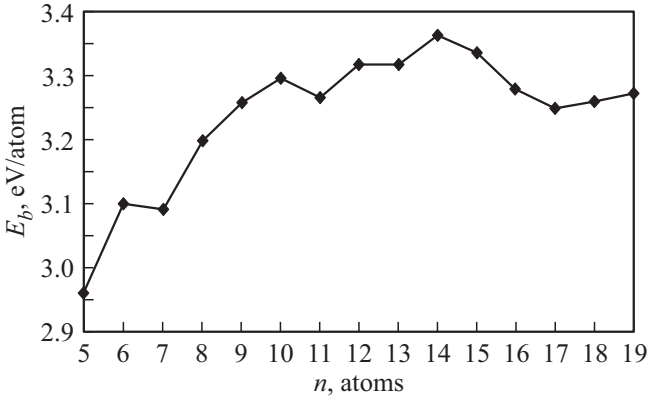

Figure 6. Graphics of the dependence of the average binding energy in the major isomers of clusters ($n = 5-19$) on the number of germanium atoms.

VGe_{19}^-. The mechanisms for the formation of stable isomers of the VGe_{19}^- cluster are analogous to the mechanisms for the formation of smaller clusters. Additional germanium atoms are added to endostructures similar to the stable isomers of the VGe_{15}^- cluster. The isomers 19-ARH1 and 19-ARH2 are closed polyhedra like the structures 15-ARH1 and 15-ARH2, with four additional germanium atoms. The isomers 19-FULL1 and 19-FULL2, similar to the isomers 17-FULL and 18-FULL, are based on a distorted fullerene-like polyhedron with sixteen vertices. In the isomer 19-FULL1, additional germanium atoms form bonds of Ge–Ge with atoms of one of the bases of the polyhedron, and in the isomer 19-FULL2 — with the atoms of the lateral surface. The isomer 19-PR is obtained by adding germanium atoms to a prismatic structure similar to the structure of the isomer 15-PR1.

According to the results of all calculations, the major isomers are 19-ARH1 and 19-ARH2. The prismatic isomer 19-PR and fullerene-like isomers 19-FULL1 and 19-FULL2 according to the results of the B3LYP calculation have slightly lower average binding energies than the major isomers, and according to the results of B3PW91 and PBE calculations, the energy separation of these structures from the major ones is large.

The experimental photoelectronic spectrum of the VGe_{19}^- cluster does not have clear features [30], while in the calculated electron spectra of stable isomers the features stand out well (Fig. 5). It can be assumed that several types of structures were detected experimentally, which led to a smoothing of the features of the photoelectronic spectrum. Figure 5 shows the total spectrum of isomers 19-ARH1 and 19-ARH2, which shows good agreement with the experimental one. There are well-defined maxima in the individual spectra of these isomers, so they correspond less to the profile of the photoelectronic spectrum.

Figure 6 shows a graph of the dependence of the average binding energy in anionic germanium-vanadium clusters on the number of germanium atoms according to the results of B3PW91 calculation. The graphs built on the basis of the results of the other two calculations do not have fundamental differences with it and therefore are not given. The expressed maximums of the average coupling energy correspond to the VGe_6^- and VGe_{14}^- clusters. The VGe_{14}^- cluster is the most stable in the series of clusters ($n = 5-19$). Given that it is also the basis for the formation of the most stable isomers of large clusters — VGe_{17}^- and VGe_{18}^-, it can be assumed that this cluster can serve as a basis for the formation of larger nanostructures.

The presented results show for the first time that the formation of clusters based on germanium can be described as part of the Wade–Mingos concept. And this applies not only to closed structures with a small number of germanium atoms, but also to large clusters, for the formation of which, as shown, building units with the structure of Wade–Mingos polyhedra are used. Therefore, Wade–Mingos rule can be used for exploratory studies of structures and other metal-germanium clusters, as well as for the predictive design of nanostructures in which such clusters are building blocks. This is especially valuable when a computer experiment is used to develop an experimental research strategy.

4. Conclusion

The structures of most stable isomers of germanium-vanadium clusters can be predicted within the $4n$-modification of Wade–Mingos rule. For a number of anion clusters VGe_n^- the major isomers of clusters with $n = 8-15$ have the structure of *arachno*-polyhedra, i.e. are obtained by removing two vertices from *closo*-polyhedra with $n + 2$ vertices. The major isomers of clusters with $n = 16-20$ are obtained by adding additional germanium atoms to the most stable arachno-structures, which are the major isomers of clusters VGe_{14}^- and VGe_{15}^-, which are the most stable in the series of clusters with $n = 5-20$.

A comparative analysis of three functionals — B3LYP, B3PW91, PBE, the most commonly used in optimization calculations of germanium-metal clusters, showed that the results obtained using the B3PW91 functional show the best agreement with experimental data. Optimization of the spatial structure using the B3LYP functional can lead to an overestimation of the relative binding energy of three-connected structures, for example, prismatic or fullerene-like, compared to deltahedral ones. The use of PBE functional for optimization calculations, on the contrary, can lead to an overestimation of the average binding energies in deltahedral structures relative to three-connected ones. To eliminate these errors, the most effective strategy for finding the major isomers of clusters is to use all three functionals, and the interpretation of the results should be carried out taking into account their features described above.

Acknowledgments

For the presented calculations, the computing resources of the Supercomputer Center of Voronezh State University were used.

Funding

The study was carried out with the support of the Ministry of Science and Higher Education of Russia within the framework of the agreement No. 075-15-2021-1351.

Conflict of interest

The authors declare that they have no conflict of interest.

References

[1] T.P. Martin, H. Schaber. J. Chem. Phys. **83**, 855 (1985).
[2] V. Kumar, Y. Kawazoe. Appl. Phys. Lett. **83**, 2677 (2003).
[3] V. Kumar, A. Kumar Singh, Y. Kawazoe. Nano Lett. **4**, *4*, 677 (2004).
[4] D. Bandyopadhyay, P. Sen. J. Phys. Chem. A **114**, *4*, 1835 (2010).
[5] M.T. Nguyen, Q.T. Tran, V.T. Tran. J. Mol. Mod. **23**, 282 (2017).
[6] X. Huang, J. Yang. J. Mol. Mod. **24**, 29 (2018).
[7] N. Du, M. Su, H. Chen. Mol. Phys. **116**, *4*, 449 (2018).
[8] Y. Zhang, J. Yang, L. Cheng. J. Clust. Sci. **29**, 301 (2018).
[9] T. Ye, Cg. Luo, B. Xu, S. Zhang, Hg. Song, Gq. Li. Struct. Chem. **29**, 139 (2018).
[10] Y.R. Zhao, T.T. Bai, L.N. Jia, W. Xin, Y.F. Hu, X.S. Zheng, S.T. Hou. J. Phys. Chem. **123**, 28561 (2019).
[11] Ben-Chao Zhu, Zhang Yu, Wang Ping, Lu Zeng, Shuai Zhang. Mater. Express **9**, *7*, 778 (2019).
[12] C. Dong, J. Yang, J. Lu. J. Mol. Mod. **26**, *85*, 84 (2020).
[13] M. Lasmi, S. Mahtout, F. Rabilloud. Comp. Theor. Chem. **1181**, 112830 (2020).
[14] V.T. Tran, Q.T. Tran. J. Comput. Chem. **41**, 31 (2020).
[15] X. Wu, Q. Du, S. Zhou, X. Huang, M. Chen, L. Miao, G. Yin, J. Wang, K. Wang, B. von Issendorff, L. Ma, J. Zhao. Eur. Phys. J. Plus **135**, 734 (2020).
[16] B. Liu, J. Yang. Mater. Today Commun. **26**, 101989 (2021).
[17] Wen-Shuai Dai, Bin Yang, Shuai-Ting Yan, Hong-Guang Xu, Xi-Ling Xu, Wei-Jun Zheng. J. Phys. Chem. A **125**, *49*, 1055 (2021).
[18] B. Liu, X. Wang, J. Yang. Mater. Today Commun. **26**, 101989 (2021).
[19] Feng Yun Zhang, C. Liu, F.L. Liu. Russ. J. Phys. Chem. B **15**, 420 (2021).
[20] X. Wang, C. Dong, J. Yang. J. Clust. Sci. **33**, 403 (2022).
[21] S.N. Khanna, P. Jena. Phys. Rev. Lett. **69**, 1664 (1992).
[22] C. Zhu, G. Yang, H. Li, D. Du, Y. Lin. Anal. Chem. **87**, 230 (2015).
[23] P. Jena, Q. Sun. Chem. Rev. **118**, 5755 (2018).
[24] Y. Jia, Z. Luo. Coord. Chem. Rev. **400**, 213053 (2019).
[25] C. Huang, H. Fang, R. Whetten, P. Jena. J. Phys. Chem. C **124**, *11*, 6435 (2020).
[26] N.A. Borshch, S.I. Kurgansky. Kondensirovannye sredy i mezhfaznye granitsy **21**, *2*, 182 (2019) (in Russian).
[27] M. Ohara, K. Koyasu, A. Nakajima, K. Kaya. Chem. Phys. Lett. **371**, *4*, 490 (2003).
[28] W. Zheng, J.M. Nilles, D. Radisic, K.H. Bowen Jr. J. Chem. Phys. **122**, 071101 (2005).
[29] K. Koyasu, J. Atobe, S. Furuse, A. Nakajima. J. Chem. Phys. **129**, 214301 (2008).
[30] J. Atobe, K. Koyasu, S. Furuse, A. Nakajima. Phys. Chem. Chem. Phys. **14**, 9403 (2012).
[31] H.G. Xu, Z.G. Zhang, Y. Feng, J.Y. Yuan, Y.C. Zhao, W.J. Zheng. Chem. Phys. Lett. **487**, 204 (2010).
[32] H.G. Xu, M.M. Wu, Z.G. Zhang, J.Y. Yuan, Q. Sun, W. Zheng. J. Chem. Phys. **136**, 104308 (2012).
[33] N. Borshch, S. Kurganskii. J. Appl. Phys. **116**, *12*, 124302 (2014).
[34] X. Wu, X.Q. Liang, Q.Y. Du, J.J. Zhao, M. Chen, M. Lin, J. Wang, G. Yin, L. Ma, R. B. King. J. Phys.: Condens. Matter **30**, 354002 (2018).
[35] N.A. Borshch, S.I. Kurgansky. Neorgan. materialy **54**, *1*, 3 (2018) (in Russian).
[36] Y.-W. Fan, H.-Q. Wang, H.-F. Li. Phys. Chem. Chem. Phys. **22**, 20545 (2020).
[37] J. Liu, P. Guo, J. Zheng, P. Zhao, Z. Jiang, L. Shen. J. Phys. Chem A **124**, 9818 (2020).
[38] J. Ulises Reveles, S.N. Khanna. Phys. Rev. B **74**, 035435 (2006).
[39] M. Shibuta, R. Takano, A. Nakajima J. Phys. Chem. C **124**, *51*, 28108 (2020).
[40] M. Shibuta, T. Inoue, T. Kamoshida, T. Eguchi, A. Nakajima. Nature Commun. **13**, *1*, 1 (2022).
[41] K. Wade. J. Chem. Soc. D **792** (1971).
[42] D.A. Mingos. Nature Phys. Sci. **236**, 99 (1972).
[43] A.D. Becke. Phys. Rev. A **38**, 3098 (1988).
[44] C. Lee, W. Yang, R.G. Parr. Phys. Rev. B **37**, 785 (1988).
[45] A.D. Becke. J. Chem. Phys. **98**, 5648 (1993).
[46] J.P. Perdew, K. Burke, M. Ernzerhof. Phys. Rev. Lett. **77**, 3865 (1996).
[47] J.P. Perdew, K. Burke, M. Ernzerhof. Phys. Rev. Lett. **78**, 1396(E) (1997).
[48] R. Ditchfield, W.J. Hehre, J.A. Pople. J. Chem. Phys. **54**, *2*, 724 (1971).
[49] R. Krishnan, J.S. Binkley, R. Seeger, J.A. Pople. J. Chem. Phys. **72**, 650 (1980).
[50] M.J. Frisch, G.W. Trucks, H.B. Schlegel, G.E. Scuseria, M.A. Robb, J.R. Cheeseman, G. Scalmani, V. Barone, B. Mennucci, G.A. Petersson, H. Nakatsuji, M. Caricato, X. Li, H.P. Hratchian, A.F. Izmaylov, J. Bloino, G. Zheng, J.L. Sonnenberg, M. Hada, M. Ehara, K. Toyota, R. Fukuda, J. Hasegawa, M. Ishida, T. Nakajima, Y. Honda, O. Kitao, H. Nakai, T. Vreven, J.A. Montgomery, Jr., J.E. Peralta, F. Ogliaro, M. Bearpark, J.J. Heyd, E. Brothers, K. N. Kudin, V.N. Staroverov, T. Keith, R. Kobayashi, J. Normand, K. Raghavachari, A. Rendell, J.C. Burant, S.S. Iyengar, J. Tomasi, M. Cossi, N. Rega, J. M. Millam, M. Klene, J.E. Knox, J. B. Cross, V. Bakken, C. Adamo, J. Jaramillo, R. Gomperts, R.E. Stratmann, O. Yazyev, A.J. Austin, R. Cammi, C. Pomelli, J.W. Ochterski, R.L. Martin, K. Morokuma, V.G. Zakrzewski, G.A. Voth, P. Salvador, J.J. Dannenberg, S. Dapprich, A.D. Daniels, O. Farkas, J.B. Foresman, J.V. Ortiz, J. Cioslowski, D.J. Fox, Gaussian. Inc., Wallingford CT, 2013.
[51] X.-J. Deng, X.-Y. Kong, H.-G. Xu, G. Feng, W.-J. Zheng. J. Phys. Chem. C **119**, *20*, 11048 (2015).
[52] Shi Shun-Ping, Liu Yi-Liang, Deng Bang-Lin, Zhang Chuan-Yu, Jiang Gang. Int. J. Mod. Phys. B **31**, 1750022 (2016).
[53] N. Huu Tho, T.T. Tu, T.M. Nhan, P.H. Cam, P.T. Thi. VNU J. Sci. Nat. Sci. Technol. **35**, *1*, 47 (2019).
[54] W. R. Wadt, P. J. Hay. J. Chem. Phys. **82**, 284 (1985).
[55] C. Siouani, S.Mahtout, S. Safer, F. Rabilloud. J. Phys. Chem. A **121**, 18 (2017).